Simultaneous Infrastructure-free Cooperative Relative Localization and Distributed Formation Control of UAVs

Kexin Guo[1], Hoang Minh Chung[1], Thien Minh Nguyen[1], Abdul Hanif Zaini[1], Lihua Xie[1] and Rodney Teo[2]

***Abstract*— This paper puts forward a simultaneous infrastructure-free cooperative relative localization (RL) and distributed formation control strategy for unmanned aerial vehicles (UAVs) in GPS denied environments. Instead of estimating relative coordinates by detecting specific patterns using image processing methods, an onboard ultra-wideband (UWB) ranging and communication (RCM) network is utilized to provide both relative distance sensing and information exchanging for RL estimation. Without any external infrastructures prepositioned, each agent cooperatively conducts the proposed consensus-based fusion method to estimate relative positions with respect to its neighbors real time though some UAVs may not have direct range measurements to their neighbors. The RL estimates together with relative velocity and inter-UAV distance measurements are applied to control a UAV swarm. Both cooperative RL and formation control are executed in a distributed way. Extensive real-world flight tests are presented to corroborate the effectiveness of our proposed simultaneous RL and formation control system.**

I. INTRODUCTION

Formation control of multi-robot systems has been a popular research topic in recent years [1]. It is one of several commonly studied motion control strategies intended for the realization of robotic swarms with many potential applications. Briefly, the aim of formation control is to organize multi-robot systems to move in a prescribed spatial pattern.

Formation experiment results, particularly those involving quadcopter UAVs, already exist, but most still depend on some external infrastructure for positioning. Examples include GPS [2], [3], motion tracking systems [4], [5], and radio-based positioning such as ultra-wideband (UWB) networks [6]. However, infrastructure dependence is disadvantageous. GPS is unreliable in cluttered urban environments, and the mentioned alternatives require careful setup in the operation area and have limited range. Even in [2], where the formation is distance-based and thus intended for use with inter-agent range measurements without infrastructure, the experiment reported was still GPS dependent.

Conversely, infrastructure-independent examples also exist, but are still deficient in some ways. In [7], a vision-based method was presented using onboard markers for relative localization (RL). Although promising, it is inherently restricted by limited view angles, occlusion and lighting, and heavy computation. In [8], a Bluetooth-based RL method was proposed and intended for collision avoidance, but experiment results show restrictions in flight duration and test area. In [9], Wang et al. formulated convex optimization-based RL. However, the method has high computational cost and thus requires centralized implementation.

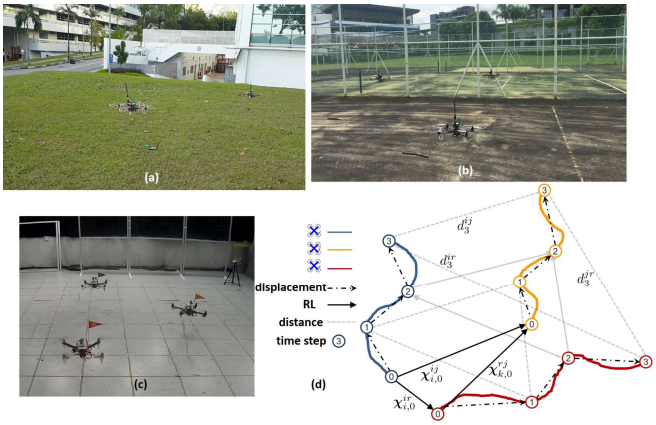

Fig. 1: **The simultaneous infrastructure-free cooperative relative localization and distributed formation shape control strategy is proposed to overcome the shortcomings of widely used global positioning and/or pattern detecting required UAV swarm applications:** (a) (b) and (c) show the distributed formation shape flights in different scenes; (d) illustrates the distances, displacements and relative position with respect to three UAVs during their simultaneous movements. For clarity, all variables are depicted at different instants.

In this paper, we present a complete autonomous multi-quadcopter system for distributed formation control utilizing infrastructure-free cooperative RL. The system is validated by both simulations and experiments on a group of three quadcopters. The RL method uses only onboard sensors and computation, and inter-agent range measurements leveraging the same UWB technology as reported in our previous works in [10], [11]. It is also cooperative, which improves performance and ensures robustness to dropouts. Unlike [2], the system here is complete, integrating RL estimates and range measurements with a suitable controller. Moreover, we propose a control algorithm which extends the work of [12] for formation shape control to the discrete case with noise and leverages the availability of both range measurements and relative positions, and group motion is governed by velocity consensus. The major contributions are:

[1]K. Guo, H. Chung, T. Nguyen, A. Zaini and L. Xie are with School of Electrical and Electronic Engineering, Nanyang Technological University, 639798, Singapore. guok0005@e.ntu.edu.sg

[2]R. Teo is with Temasek Laboratories, National University of Singapore, 117411, Singapore.

- A cooperative RL strategy independent of infrastructure using only onboard sensors and inter-agent ranging. The RL estimation is bounded with consideration of noise;
- A consensus-based RL fusion to enhance robustness to dropouts. Experiment results verify the effectiveness of this approach;
- A distributed distance-based formation control law using RL estimates and range measurements. Bounded convergence of the algorithm with noise is provided;
- A formation of real quadcopter UAVs demonstrating the complete system of RL and formation control utilizing a customized UWB ranging and communication (RCM) network.

To keep the paper brief, only proof sketches are provided. Detailed analysis will be provided in the extended journal version.

The organization of this paper is as follows: first the problem formulation is introduced in Section II. Then we propose a UWB network based RL initialization strategy followed by consensus-based RL fusion in Section III. Section IV discusses a discrete-time formation control algorithm by using the RL estimates. Flight experiments are conducted in Section VI and the conclusion is summarized in Section VII.

II. Problem of Interest

Consider a UAV team consisting of N agents working collaboratively to localize themselves with respect to their neighbors and conduct formation control simultaneously. Denote by $\mathcal{N}_i$ the UAVi's neighbor set in which it can achieve the distance measurement d^{ij} and receive data packets from UAVj for $j \in \mathcal{N}_i$. Leveraging on this sensing information, UAVi aims to estimate the relative coordinates $\boldsymbol{\chi}_{i,k}^{ij}$ with respect to UAVj at $t = t_{i,k}$ in UAVi's own frame $\mathcal{F}_i$ as depicted in Figure 1(d). Note that two scenarios are considered here: (1) UAVi is able to sense UAVj and conduct RL estimation directly, i.e., UAVj is a primary node for UAVi; (2) UAVi is only able to range and communicate with UAVr which is a neighbor of UAVj, but fails to sense UAVj directly, and UAVj herein serves as a secondary node. The first objective is to develop a RL estimator such that each UAVi can estimate $\boldsymbol{\chi}_{i,k}^{ij}$ within its neighbor set. With these RL estimates and inter-UAV distance measurements, the next objective is to design a distributed distance-based formation control for real-world UAV swarm applications.

III. Consensus-based Cooperative Relative Localization

In this section, we first present a RL initial estimation strategy based on UWB RCM network and then two local RL estimators are introduced with consideration for noise. To enhance the robustness of our RL estimation, we propose a consensus-based RL fusion method to fuse the local RL estimates.

A. RL Initialization

In this section a non-linear regression (NLR) based method [6] is applied to estimate the coordinates of the static UAVs before they take off, and these estimates will serve as an intial guess of the RL estimators in Section III-B to improve RL accuracy. For a network with N UAVs, we will group these coordinates into one vector as $\boldsymbol{p} = \begin{bmatrix} x_1 & y_1 & z_1 & x_2 & y_2 & z_2 & \dots & x_N & y_N & z_N \end{bmatrix}^T$. In the context of a non-linear regression problem, the known coordinates will be in the set of error-free independent variables $\boldsymbol{x}$ and the unknown will be in the set of parameters $\boldsymbol{\phi}$ to be estimated.

Our non-linear model $f(\boldsymbol{x},\boldsymbol{\phi})$ is a $N(N-1)/2 \times 1$ vector of all of the distances arranged in a particular way as follows $\begin{bmatrix} d_0^{12} & d_0^{13} \dots d_0^{1N}, & d_0^{23} & d_0^{24} \dots d_0^{2N}, \dots, d_0^{N-1,N} \end{bmatrix}^T$.

The observed dependent variables $\underline{d}^{ij}$ are these distances subject to some noise ϵ^d, or $\underline{d}^{ij} = d^{ij} + \epsilon^d$. $\underline{\boldsymbol{d}}$ is a stack of all distance measurements $\underline{d}^{ij}$. To apply the non-linear regression method, we start from some initial guess $\boldsymbol{\phi}_0$ and seek to improve our estimate of $\boldsymbol{\phi}$ by the following recursive steps:

$$\boldsymbol{J}_k = \boldsymbol{J}_k(\boldsymbol{x}, \boldsymbol{\phi}_k) = \left.\frac{\partial f(\boldsymbol{x}, \boldsymbol{\phi})}{\partial \boldsymbol{\phi}}\right|_{\boldsymbol{\phi}=\boldsymbol{\phi}_k} \tag{1a}$$

$$\Delta\underline{\boldsymbol{d}} = \underline{\boldsymbol{d}} - f(\boldsymbol{x}, \boldsymbol{\phi}_k) \tag{1b}$$

$$\Delta\boldsymbol{\phi} = (\boldsymbol{J}_k^T \boldsymbol{W} \boldsymbol{J}_k)^{-1} \boldsymbol{J}_k^T \boldsymbol{W} \Delta\underline{\boldsymbol{d}} \tag{1c}$$

$$\boldsymbol{\phi}_{k+1} = \boldsymbol{\phi}_k + \Delta\boldsymbol{\phi} \tag{1d}$$

where $k = 0, 1, 2, 3...$ and $\boldsymbol{W}$ is a weight matrix to signify the comparative importance between the measurements.

Remark III.1 *The local referential system is somewhat arbitrary; the polygon can be translated and rotated as needed by the user. Thus, for a three-UAV team, UAV*0 *can be simply defined as the origin, UAV*1 *is set along the $x-$axis (its y value assigned to zero), and all the UAVs' heights z can be set as zero during the initial phase [13]. These mild initial settings constrain the system to three unknowns for regression for a group of 3 UAVs. In our work, this RL initialization method has been simulated and shown to be feasible. To apply this technique, a UWB RCM scheme is developed in Section VI.*

B. RL of Mobile UAVs

1) Persistent Excitation-based RL Estimation : Suppose each UAVi is able to measure the relative distance d_k^{ij} of its neighbor j at sampling time instants $t_{i,k}$. Meanwhile, UAVi will transmit certain information to its neighbors (e.g., UAVj) including $\boldsymbol{v}_{i,k}$, local RL estimates, etc, by decoding the data packet entrained in one ranging request command. Although UAVj can acquire its own velocity $\boldsymbol{v}_{j,t}$ continuously, the sampled value $\boldsymbol{v}_{j,k}$ at $t = t_{j,k}$ is actually chosen for calculation once $\boldsymbol{v}_{i,k}$ received. Note, however, that the larger the data packet the longer the time duration for one ranging slot and thus, practically, a trade-off between ranging precision and the quantiy of data transmission should be considered precedently for a UWB RCM protocol design. We aim to design an estimator for each UAV in a certain team based on the available information to localize the relative position $\boldsymbol{\chi}^{ij}$ in its own local frame (i.e., j's relative coordinate in i's moving frame at $t = t_{i,k}$ is $\boldsymbol{\chi}_{i,k}^{ij}$).

Since all quadcopters carry compasses, the orientations of reference frames $\mathcal{F}_i$ and $\mathcal{F}_j$ for $i \neq j$ are consistent, it follows that $\boldsymbol{\chi}_{k+1}^{ij} = \boldsymbol{\chi}_k^{ij} + T\boldsymbol{\nu}_k^{ij}$ where T is the sampling interval, and the duality of the RL problem illustrates $\boldsymbol{\chi}_{i,k}^{ij} = -\boldsymbol{\chi}_{j,k}^{ji}$. Taking the derivative of both sides of $d_t^{ij^2} = ||\boldsymbol{\chi}_t^{ij}||^2$ with respect to time in continuous-time version and we can get $d_t^{ij}\dot{d}_t^{ij} = \boldsymbol{\nu}_t^{ij^T}\boldsymbol{\chi}_t^{ij}$. By discretizing it, one obtains $d_k^{ij}\dot{d}_k^{ij} = \boldsymbol{\nu}_k^{ij^T}\boldsymbol{\chi}_k^{ij}$. By taking into account the sensor noise, the RL estimation from UAVi at $t = t_{i,k+1}$ is written as (2).

$$\hat{\boldsymbol{\chi}}_{i,k+1}^{ij} = \hat{\boldsymbol{\chi}}_{i,k}^{ij} + T\underline{\boldsymbol{\nu}}_{i,k}^{ij} + \gamma T\underline{\boldsymbol{\nu}}_{i,k}^{ij}\left(\underline{d}_k^{ij}\underline{\dot{d}}_k^{ij} - \underline{\boldsymbol{\nu}}_{i,k}^{ij^T}\hat{\boldsymbol{\chi}}_{i,k}^{ij}\right) \tag{2}$$

where $\underline{\boldsymbol{\nu}}_{i,k}^{ij}$, $\underline{d}_k^{ij}$ and $\underline{\dot{d}}_k^{ij}$ are the measurements of $\boldsymbol{\nu}_{i,k}^{ij}$, d_k^{ij} and $\dot{d}_k^{ij}$ respectively at the kth time step. $\gamma \in \mathbb{R}^+$ is a tuneable constant gain. Bounded RL estimation in noise-corrupted case can be proved and due to the space limitation, the complete proof will be shown in our extended version. Note that the *underline* of each variable throughout this paper presents its corresponding measurement.

2) Filter-based RL Estimation: An EKF structure is proposed herein to account for the noise of the difference of the increment of UAVs' displacements and their relative distances. The state space consists of relative position $\boldsymbol{\chi}_k^{ij}$ and relative velocity $\boldsymbol{\nu}_k^{ij}$, with the system dynamics given as follows:

$$\begin{cases} \boldsymbol{\chi}_{k+1}^{ij} = \boldsymbol{\chi}_k^{ij} + \boldsymbol{\nu}_k^{ij} \cdot T + \frac{1}{2}\boldsymbol{\varrho}_k^{ij}T^2, \\ \boldsymbol{\nu}_{k+1}^{ij} = \boldsymbol{\nu}_k^{ij} + \boldsymbol{\varrho}_k^{ij}T, \end{cases} \tag{3}$$

where $\boldsymbol{\varrho}_k^{ij}$ is the acceleration difference between UAVi and UAVj at $t = t_k$. In the case when the acceleration is not available, $\{\boldsymbol{\varrho}_k^{ij}\}$ can be treated as a white noise sequence with the covariance $\mathbb{E}(\boldsymbol{\varrho}_k^{ij}\boldsymbol{\varrho}_k^{ij^T}) = \text{diag}(\sigma_x^2, \sigma_y^2, \sigma_z^2)$. Note that σ_* can be set as the maximum acceleration on the $*$-direction ($* = x, y, z$) for a conservative but consistent estimation.

The observations are the relative range $\underline{d}_k^{ij}$ and relative velocitiy $\underline{\boldsymbol{\nu}}_k^{ij}$ between UAVi and UAVj as below:

$$\begin{cases} \underline{d}_k^{ij} = ||\boldsymbol{\chi}_k^{ij}|| + \eta_{r,k}, \\ \underline{\boldsymbol{\nu}}_k^{ij} = \boldsymbol{\nu}_k^{ij} + \boldsymbol{\zeta}_{\boldsymbol{\nu}^{ij},k}, \end{cases} \tag{4}$$

Assume that both the process and measurement noises are Guassian white noise. Finally, a standard Kalman filter is conducted after linearizing the measurement equation.

Consider a team of m homogeneous UAVs. Each UAV $\mathcal{F}_i$ features m-1 EKF estimators to keep track of the other members' relative position and uses their outputs to determine its formation control command as seen in Section IV.

Convergence time of EKF has to be considered for real flight tests. Unreasonable RL estimates before convergence of EKF may cause our system to move dramatically or even crash. Thus, in real applications an autonomous initialization method III-A is conducted prior to the RL estimator. The intial RL guess will be fed into our proposed RL estimator III-B.1 and III-B.2. These two estimators are executed simultaneously, and due to the robusness to sensor noise, the estimates from EKF based estimator will be utilized for control if the error covariance of the estimates is acceptable (less than a certain threshold). RL estimation (2) can serve as an excitation estimator, when the deviation of EKF based estimator is large or even diverges (i.e. caused by outliers or instant large maneuvering), to provide emergency information to guarantee a basic and safe flight as well as recover the EKF based estimator.

C. Consensus-based RL Fusion

In the presence of unexpected disturbances such as wind, one UAV may suddenly change its trajectory at some time step such that the true relative positions to other regular moving UAVs will be changed hugely. In this paper, a consensus-based fusion procedure is proposed to mitigate this potential danger by fusing the direct and indirect RL estimates as described in Section II. The proposed fusion strategy is able to make the RL estimation error less violent, i.e., the error curve is smooth around the upper bound even at the instant where the unexpected change occurs. The details are introduced as follows.

Based on the bounded estimation of a local RL estimator, $\lim_{k\to\infty} ||\tilde{\boldsymbol{\chi}}_k^{ij}|| \leq c$ is achieved from (2)-(4) for each UAV where c is the upper bound of the RL estimation error. Inspired by the equation (8) in [14], we consider a noise-corrupted consensus-based RL fusion strategy as (5).

$$\begin{aligned} \boldsymbol{\pi}_{i,k+1}^{ij} =& \boldsymbol{\pi}_{i,k}^{ij} + T\underline{\boldsymbol{\nu}}_{i,k}^{ij} + b_{ij}\left[\hat{\boldsymbol{\chi}}_{i,k}^{ij} - \boldsymbol{\pi}_{i,k}^{ij}\right] \\ &+ \sum_{r\in\mathcal{N}_i\setminus\{j\}} a_{ir}\left[\hat{\boldsymbol{\chi}}_{r,k}^{ij} - \boldsymbol{\pi}_{i,k}^{ij}\right] \end{aligned} \tag{5}$$

where $\hat{\boldsymbol{\chi}}_{r,k}^{ij}$ is an indirect relative estimate obtained by UAVi through an intermediate UAVr and $\hat{\boldsymbol{\chi}}_{r,k}^{ij} = \hat{\boldsymbol{\chi}}_{i,k}^{ir} + \boldsymbol{\pi}_{r,k}^{rj}$. The fused RL estimate $\boldsymbol{\pi}_i^{ij}$ in (5) will asymptotically converge to the relative coordinate $\boldsymbol{\chi}^{ij}$ with a bounded estimate error. The details of proof will be found in our future work due to page restrictions.

IV. Distributed Formation Control

In this section, a distributed formation control integrated with RL estimates is proposed and its discrete-time case with noise is applied for real-world flights in Section VI-D. The complete system workflow is summarized as follows.

A. Formation Control Design using RL Estimates

In [12], a continuous-time algorithm that combines flocking and distance-based shape control is proposed and a double-integrator model of the system is given. However, in our cases, this continuous-time version cannot be implemented directly since the UWB RCM network only allows UAVi ranging and talking to its neighbors for a time period T and then conducting a RL estimate at the end of each such interval. This section adopts a discrete-time algorithm that combines the proposed relative localization estimates with distance-based formation shape control, where the distance and relative velocity measurements are considered being

contaminated by Gaussian noise. The discrete-time formation control implemented on UAVi with noises is given by

$$\begin{aligned}\boldsymbol{p}_{i,k+1} =& \boldsymbol{p}_{i,k} + T\boldsymbol{v}_{i,k} \\ \boldsymbol{v}_{i,k+1} =& \boldsymbol{v}_{i,k} + \gamma_1 TK \sum_{j\in\mathcal{N}_i} \underline{\boldsymbol{\nu}}_k^{ij} + \gamma_2 T \left[\sum_{j\in\mathcal{N}_i} \left(\underline{d}_k^{ij\,2} - d_{ij}^{*2}\right) \boldsymbol{\pi}_{i,k}^{ij}\right]\end{aligned} \tag{6}$$

where K is the consensus gain, γ_1 and γ_2 are small positive constants, and d_{ij}^* is the desired relative distance between UAVi and UAVj. Note that the relative position term in (6) adopts our RL estimate $\boldsymbol{\pi}_{i,k}^{ij}$. Here the proof on convergence is omitted and the details of proof can be found in our journal version.

B. Algorithm Realization

The preceding two subsections III-B and III-C present the proposed distributed cooperative RL estimator and consensus-based fusion method respectively. Persistent excitation (PE) based RL method in Section III-B.1 is robust to the intial RL estimates while the EKF-based estimator in Section III-B.2 is a bit sensitive to the initial guess especially in the case where the initial RL guess is quite far from the true relative position, but on the other hand, considering the disturbance rejection ability, the accuracy of RL estimates from persistent excitation-based RL is proportional to the magnitude of sensor noises. Thus, in the practical applications, we propose to combine these two methods to make full use of their respective strengths. PE-based method can aid EKF-based estimator when it significantly deviates from the true value or even diverges. The fused RL estimates from Section III-C will enhance the robustness of RL estimation especially in presence of unexpected maneuverings of a certain UAV. The details of our proposed RL algorithm are presented in Algorithm 1. Here we use left subscripts ${}_{pe}\hat{\boldsymbol{\chi}}$ and ${}_{ekf}\hat{\boldsymbol{\chi}}$ to distinguish the RL estimates obtained from Section III-B.1 and Section III-B.2.

Algorithm 1: Pseudocode for RL $\boldsymbol{\pi}_{i,k}^{ij}$ Estimation

Procedure: RL Initialization
Ranging and communication, then conduct NLR:
  while $\Delta\boldsymbol{\phi} > \kappa$ **do**
    for $i \leftarrow 1$ *to* N **do**
      if $i == N$, $j \leftarrow 0$; otherwise $j \leftarrow i+1$
      UAVi sends range request and data package to UAVj
      Calculate the relative distance $\underline{d}_k^{ij}$
    $\boldsymbol{J}_k \leftarrow (1a)$, $\Delta\underline{\boldsymbol{d}} \leftarrow (1b)$, $\Delta\boldsymbol{\phi} \leftarrow (1c)$, $\boldsymbol{\phi}_{k+1} \leftarrow (1d)$
Each UAV stores the initial RL estimates $\hat{\boldsymbol{\chi}}_0^{ij} \leftarrow (\boldsymbol{x}, \boldsymbol{\phi})$
Procedure: Cooperative RL Estimation
while $CooperativeRL$ **do**
  for $i \leftarrow 1$ *to* N **do**
    if $i == N$, $j \leftarrow 0$; otherwise $j \leftarrow i+1$
    UAVi sends range request and data package to UAVj
    Calculate the relative distance $\underline{d}_k^{ij}$ and indirect relative velocity measurement $\underline{\boldsymbol{\nu}}_k^{ij}$
    ${}_{pe}\hat{\boldsymbol{\chi}}_{i,k+1}^{ij} \leftarrow (2)$
    ${}_{ekf}\hat{\boldsymbol{\chi}}_{i,k+1|k}^{ij}, \hat{\boldsymbol{\nu}}_{i,k+1|k}^{ij} \leftarrow (3)$
    conduct EKF procedure referring to [10]
    update ${}_{ekf}\hat{\boldsymbol{\chi}}_{i,k+1}^{ij}$ and $\boldsymbol{P}_{i,k+1}$
    if $||\boldsymbol{P}_{i,k+1}|| < \tau$ **then**
      output ${}_{ekf}\hat{\boldsymbol{\chi}}_{i,k+1}^{ij}$
    else
      ${}_{ekf}\hat{\boldsymbol{\chi}}_{i,k+1}^{ij} \leftarrow {}_{pe}\hat{\boldsymbol{\chi}}_{i,k+1}^{ij}$, reset $\boldsymbol{P}_{i,k+1}$
    $\hat{\boldsymbol{\chi}}_{i,k+1}^{ij} \leftarrow {}_{ekf}\hat{\boldsymbol{\chi}}_{i,k+1}^{ij}$, $\boldsymbol{\pi}_{i,k+1}^{ij} \leftarrow (5)$
Calculate the control command $\leftarrow (6)$
Send command to flight control board

V. Numerical Simulations

A. Simulation of RL Initialization

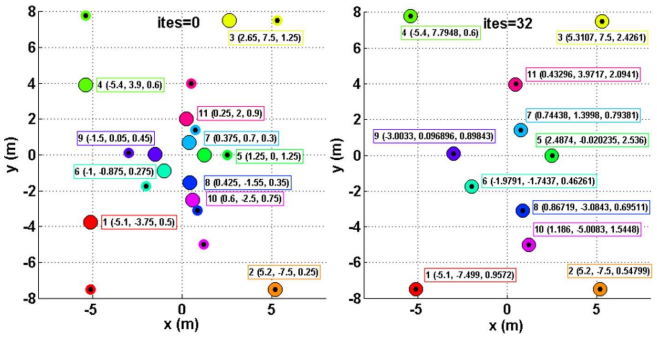

Fig. 2: The output of the NLR algorithm to estimate the coordinates of 11 UAVs after 32 iterations. The current estimated location of the UAVs are marked by the larger coloured circles. The true location of a UAV is marked by a smaller circle of the same colour but with a black centre.

In this section we present a simulation on the the use of NLR algorithm to estimate the positions of UAVs on start-up where all of them are static. In Table I, the true coordinates of the UAVs are listed. We choose to fix the x coordinates of UAV1 and 2, y coordinates of UAV2 and 3, and x and z coordinates of UAV4 since they are at the farthest extents of the localization area. In this simulation we also added a random Gaussian noise with standard deviation $0.05m$ into the distance measurements which is the documented specification of the UWB device by the manufacturer. For 3 UAVs, the coordinates can be initialized as Remark III.1. The results of the NLR algorithm in the beginning and after 32 iterations are shown in Figure 2. From a very poor initial guess, it can be seen that only after 32 iterations the x and y estimates are almost the same with the true values.

B. Cooperative RL Simulation Results

Six mobile UAVs are involved in this section with the sensing graph depicted in Figure 3(a). UAV2, 3 and 4 have

TABLE I: True positions of the agents, the numbers in bold are the fixed values $\boldsymbol{x}$.

UAV	x	y	z	UAV	x	y	z
01	**-5.1**	-7.5	1	07	0.75	1.4	0.6
02	**5.2**	**-7.5**	0.5	08	0.85	-3.1	0.7
03	5.3	**7.5**	2.5	09	-3	0.1	0.9
04	**-5.4**	7.8	**0.6**	10	1.2	-5	1.5
05	2.5	0	2.5	11	0.5	4	1.8
06	-2	-1.75	0.55				

direct range measurements to UAV1 while UAV5 and 6 can only have indirect estimate through their neighbors. To demonstrate the proposed RL estimation scheme, we set UAV1 as a relative target to estimate since it is globally reachable due to the sensing graph. In the simulation, UAV4 conducts a sudden velocity deviation at $t = 100s$ as shown in Figure 3(b). Distance noise and velocity noise are considered as Gaussian white noise with $N(0, 0.1^2)$ and $N(0, 0.2^2)$. Choose $T = 0.05s$, $\gamma = 0.5$, $b_{ij} = \frac{\alpha_{ij}}{|\mathcal{N}_i|+1+\alpha_{ij}}$ and $a_{ij} = \frac{1}{|\mathcal{N}_i|+1+\alpha_{ij}}$ where $|\mathcal{N}_i|$ is the cardinality of $\mathcal{N}_i$, and $\alpha_{ij} = 1$ if UAVi has a direct measurement of UAVj, and $\alpha_{ij} = 0$ otherwise. Therefore, every UAV has its own local estimate $\boldsymbol{\pi}_i^{i1}$, $i = 2, \ldots, 6$ and these RL estimates converge to the true relative coordinates as shown in Figure 3(d). The evolution curves of the estimation errors $||\boldsymbol{\pi}_{i1} - \boldsymbol{\chi}_{i1}||$ are depicted in Figure 3(c) and converge within a bound of $0.21m$. Note that, in Figure 3(c), the fused estimates $\boldsymbol{\pi}_{31}$, $\boldsymbol{\pi}_{51}$ and $\boldsymbol{\pi}_{61}$ fluctuate slightly in the presence of a big variance of $\boldsymbol{\pi}_{41}$ at $t = 100s$, and this demonstrates that our proposed cooperative RL method is robust to unexpected maneuverings.

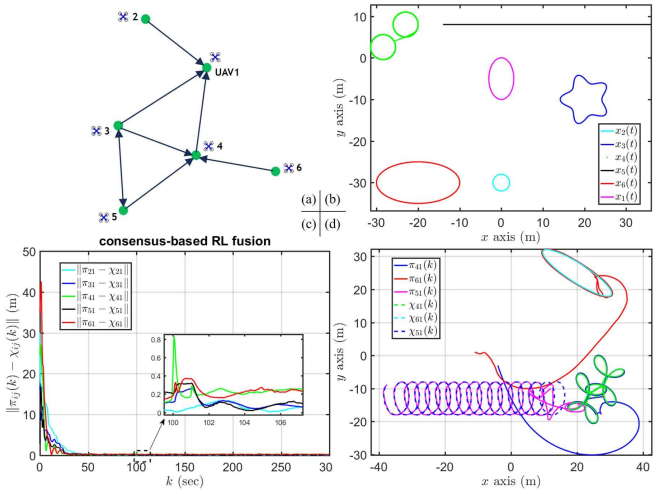

Fig. 3: **RL estimation results with sudden change of the path of UAV**4: (a) the sensing graph; (b) trajectories of six UAVs; (c) the evolution of RL estimation error $\|\boldsymbol{\pi}_{i1} - \boldsymbol{\chi}_{i1}\|$ calculated on UAVi, $i = 2, \ldots, 6$; (d) comparison between fused RL estimates and true values in x-y plane.

C. Combining Cooperative RL and Formation Control

Consider a three-UAV team where each UAV can measure the distance to the other two UAVs. The control goal is to form two triangular formation shapes with velocity consensus by utilizing the RL estimates. In the simulation, we set $K = 1$, $\gamma_1 = 1$, $\gamma_2 = 1.4 \times 10^{-2}$, and adopt the same parameters of RL estimation introduced in Section V-B. In addition, we set the maximum flight velocity is $5m/s$, formation error is $1m$ and the velocity consensus error is $0.5m/s$. Note that here we use fused RL estimate $\boldsymbol{\pi}_{i,k}^{ij}$ generated from Algorithm 1 for our formation control and two equilateral triangular formation shapes are preconfigured with side length of $d_{ij}^* = 15m$ and $30m$ sequentially.

Compared with the noiseless case (without distance and velocity noises and using true relative position, see Figure 4(a)), in Figure 4(b), two equilateral triangular formation shapes are formed in succession and sustained by using noisy distance and velocity measurements, as well as RL estimates. Due to the introduction of noise, the UAV team has to keep updating formation control commands and maintaining the formation, and thus the flight trajectories in Figure 4(b) are not perfect as Figure 4(a). The desired two formations are achieved at $11s$ and $15s$ respectively and the inter-UAV distances are maintained at $30m$ finally as shown in Figure 4(c). From Figure 4(d), we observe that both of these two cases achieve velocity consensus where the fluctuations of relative velocities in the beginning indicate the switch of two desired formations.

VI. Flight Experimental Evaluations

In this section we present extensive flight experimental evaluations to demonstrate our proposed simultaneous cooperative RL and distributed formation shape control system. At first the performance of cooperative RL is evaluated in terms of average absolute error with comparison of VICON® ground truth (a motion capture system with milimeter-level positioning accuracy). Then, this cooperative RL combined with the proposed distributed formation shape control is demonstrated by three-quadcopter flights. Actually, numerous simulations of both RL estimation and combined formation shape control have been carried out before starting the flight experiments and the corresponding results are omitted here due to page restrictions.

A. System Configurations

Figure 5 illustrates the hardware configuration and signal flow of the UWB based RL system. UWB modules PulsON 440® were installed on three quadcopters. Due to the large bandwidth (from 3.1 GHz to 5.3 GHz), UWB is robust to multipath and non-line-of-sight effects, and provides a reliable long distance ranging with an accuracy within $10cm$. All of the algorithms, sensing and communication drivers are exectuted on a credit-card sized mobile-level Raspberry Pi2® with an ultra-low power processor ARM Cortex-A7 running at 900MHz. The quadcopter is equipped with Pixhawk®, integrating inertial measurement unit and flight controller on board, as well as Px4Flow® for onboard velocity estimation. Note that other equivalent velocity or displacement sensing systems can be adopted as well. The UWB module on each quadcopter actively sends ranging requests to neighboring

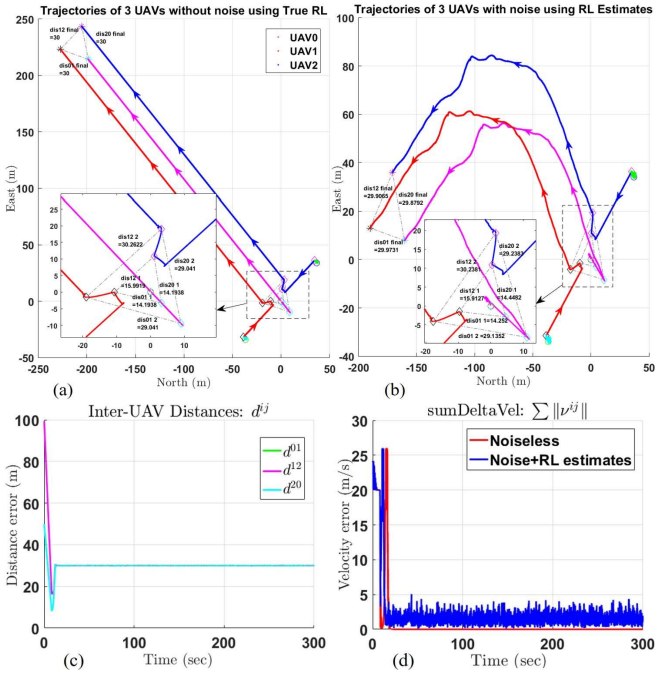

Fig. 4: **Simulation results of formation control using RL estimates in noise-corrupted case and the system dynamics are governed by (6)**: (a), (b) show the flight trajectories of 3 UAVs using true RL in noise-free conditions, and using RL estimats in noise-corrupted case respectively; (c) depicts the evolutions of inter-UAV distances; (d) presents sum of the 2-norm of the relative velocities: noiseless distance measurements + true RL (red) and noisy distance measurements + RL estimates (blue).

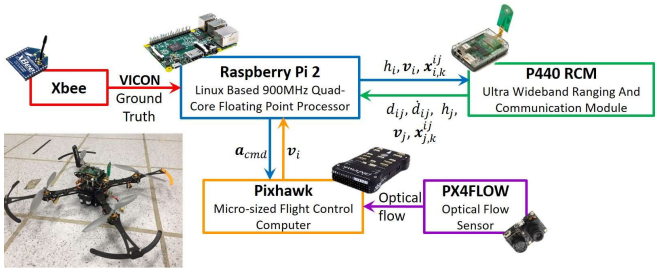

Fig. 5: Flight platform and diagram of system workflow.

UAVs for distance measurement and communication based on the two-way time of flight (TWToF) ranging method and a customized network protocol introduced in Section VI-B. In this UWB RCM network, an instant distance estimate obtained by UAVi will be calibrated through linear regression and its corresponding parameters have been determined by a series of experiments in different environments [10]. This corrected range together with the received information then goes through the outlier detection before it is stored in the database. To reduce the computation and avoid excessive repetition of similar data, only selected distance measurements and neighbor's information are recorded and stored.

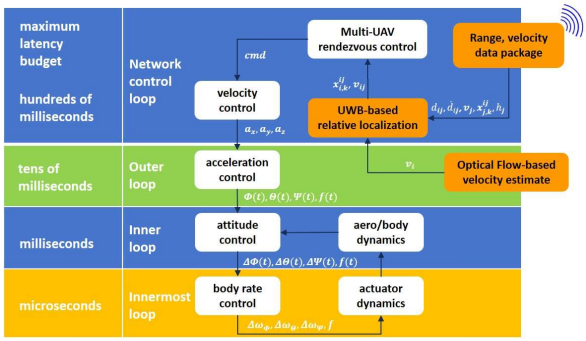

Fig. 6: Diagram of flight control workflow

TABLE II: TDMA slotmap configuration for 3 UAVs

Slot	Requester ID	Responder ID	Data package (16 bytes)
01	200	201	yes
02	201	202	yes
03	202	200	yes

Note that the RL initialization algorithm is processed first and its output serves as the initial state estimate for PE- and EKF-based RL estimators. Finally, the fused RL estimate update will be fed into the flight controller for quadcopter navigation as depicted in Figure 6. All the processes above are controlled by Raspberry Pi2® and XBee® only receives each UAV's global position and velocity from VIOCN as ground truth.

B. Ultra-wideband Ranging and Communication Network Configuration

A contention-free Time Division Multiple Access (TDMA) time-slotted network is used to coordinate communications and range measurements. The basic mechanism of TDMA is a common network clock which is used to drive an airtime slotmap. In addition, each node transmits its previous range and velocity of range measurement provided by UWB firmware, together with its current velocity estimate as data embedded in the range request packet. All nodes overhear this data and optionally provide it to a co-located host processor. An example of a slot map supporting three network nodes, with unique identifiers $200-202$ (i.e., UAV0-2) is given in Table II. Each slot supports a TWToF range conversation with associated data package. On completion of slot 3, the process will repeat from slot 1.

C. Experimental Evaluations of RL Estimation

To verify our proposed RL system, on-board tests were carried out on three simultaneous moving UAV platforms at Internet of Things lab as seen in Figure 1(c) where a VICON system is installed for the ground truth. Each UAV concurrently conducts ranging measurement and communicates its local estimates with its neighbors. Meanwhile, our proposed Algorithm 1 will be executed at the end of each communication in a distributed way.

In order to cover distinct situations, 13 tests were conducted with different speeds and travelling patterns including **S**tatic, **C**ircle, **T**riangle, **L**ine, random **W**alk and **NTU** letters.

Since the RL performances of these three UAVs are similar, without losing generality, here we show the average absolute RL estimation errors of UAV2 as an example in Table III where 2**S**1**C**_2 means the second test with two UAVs being static and one moving in a circle. The statistical results illustrate that the mean of our proposed RL estimation error along one axis is around $0.2m$ in the presence of distance and velocity measurement noises.

TABLE III: Average absolute RL estimation errors $\frac{1}{n}\sum_{i=1}^{n}|\hat{x}_i - x_i^{GT}|$ calculated on UAV2. (Unit:m)

Test	$\hat{\chi}_2^{01}-\chi^{01}$		$\hat{\chi}_2^{12}-\chi^{12}$		$\hat{\chi}_2^{20}-\chi^{20}$	
	$\lvert\delta x\rvert$	$\lvert\delta y\rvert$	$\lvert\delta x\rvert$	$\lvert\delta y\rvert$	$\lvert\delta x\rvert$	$\lvert\delta y\rvert$
01_2**S**1**C**_1	0.132	0.110	0.141	0.098	0.121	0.111
02_2**S**1**C**_2	0.150	0.101	0.136	0.122	0.141	0.118
03_2**S**1**T**_1	0.245	0.117	0.230	0.155	0.237	0.122
04_2**S**1**T**_2	0.258	0.133	0.249	0.148	0.234	0.161
05_1**S**2**C**_1	0.267	0.120	0.233	0.123	0.244	0.131
06_1**S**2**C**_2	0.296	0.094	0.261	0.103	0.266	0.139
07_1**S**2**T**_1	0.202	0.167	0.215	0.187	0.216	0.151
08_1**S**2**T**_2	0.227	0.115	0.212	0.176	0.249	0.133
09_1**L**2**C**	0.190	0.186	0.197	0.189	0.201	0.182
10_3**W**	0.203	0.223	0.210	0.216	0.219	0.206
11_3**T**	0.217	0.204	0.215	0.216	0.205	0.221
12_3**C**	0.247	0.220	0.218	0.237	0.232	0.226
13_**NTU**	0.222	0.190	0.211	0.208	0.238	0.198
mean	**0.219**	**0.152**	**0.210**	**0.167**	**0.215**	**0.161**

Figure 7(d) illustrates the plot of overhead 2-D trajectory recorded on UAV2 from Test no.13. It can be seen that the average absolute RL estimation errors in x and y directions are less than $0.4m$ with the worst case. Since the RL estimation is conducted distributively, the RL estimation errors generated on each UAV have the same magnitude even though there exist slight differences between each pair of UAVs. Without loss of generality, the evolution curves of RL trajectories and estimation errors on UAV2 are shown in Figure 7(a).

D. Quadcopters Formation Flight

In this section, we implemented the proposed distributed formation control utilizing cooperative RL on quadcopters with the same configuration as described in Section VI-A, and conducted a series of real-world flight tests in a grass field at Nanyang Technological University and an abandoned basketball court near Science Center Singapore. These outdoor experiments also demonstrate the robustness of the systems against wind disturbances. In both these fields, an equilateral triangle formation of 3 UAVs was achieved successfully[1].

There are three UAVs involved in the experiments, which comprise of one leader (UAV1) and two followers (UAV0 and 2). The control of these UAVs are set in a global coordinate frame with x-axis align with magnetic East and y-axis with magnetic North. Initially, all three UAVs are placed on the ground, roughly following a pre-defined configuration for consistency purpose. In particular, we assign UAV0 as a launching origin and place UAV1 along the East direction with respect to UAV0 in order to keep the flight control coordinate and the RL coordinate system consistent. Meanwhile, UAV2 can be put arbitrarily in North zone. Uppon power-startup, the UWB modules will measure the distances and start communication, and the Raspberry Pi2® would then derive initialization configuration and start estimating relative positions. With estimated relataive positions, control outputs can be calculated accordingly. Secondly, when on-board control outputs are available for all UAVs, there pilots would then manually takeoff and ascend the UAVs to $1.5m$ altitude, with respect to terrain. This altitude is chosen to minimize ground aerodynamic disturance while maintaining good visual contact for the optical flow velocity estimator. When the target altitude is reached, two pilots would then switch their UAVs, from manual flight mode, to formation flight mode, where the UAV would automatically control its velocity to satisfy formation requirements. One pilot, controlling the leader UAV1 would then manually fly the UAV in predefined trajectories to test the behavior of follower UAVs. If the follower UAVs could automatically maintain the predefined shape formation against unknown movements from leader UAV, the experiment is considered sucessful. A flight video snapshot is shown in Figure 8, where three UAVs reach the desired formation of an equilateral triangle with side length of $3m$ and maintain the formation with the movements of the leader UAV. Online inter-UAV distance measurements and the relative bearing evolutions in the process of forming the desired formation shape, are depicted in Figure 9(a) and 9(b), where three different background colors respectively show the launching, formation keeping and landing phase. After a period of adjustment, the desired formation shape is achieved and kept from $56s$ to $257s$ with $3m$ relative distance and 60° relative azimuth angle.

[1]Flight video can be found in: `https://youtu.be/vqZH_BoMy8U`

VII. Conclusion

This paper proposes a combined distributed cooperative RL and distance-based formation control scheme for UAV swarms without infrastructures and global positions. Based on the capability of the designed UWB RCM network, each UAV is able to estimate the relative positions of its neighbours by utilizing our proposed consensus-based RL fusion scheme. These RL estimates combined with the inter-UAV distances and relative velocity estimates are directly fed into our designed discrete-time distributed formation control law to achieve formation flights. Extensive flight experiments verify the effectiveness of our proposed system. The cooperative RL and formation control with applications to mobile vehicles in frame-free case will be investigated in our future work.

Acknowledgment

The authors would like to thank Dr. Shuai Liu, Dr. Duo Han and Dr. Xiuxian Li for their theoretical supports, and Mr. Tete Ji, Mr. Muqing Cao and Mr. Ren Xiang Foo for their assistance in numerous experiments.

References

[1] K.-K. Oh, M.-C. Park, and H.-S. Ahn, "A survey of multi-agent formation control," *Automatica*, vol. 53, pp. 424–440, 2015.

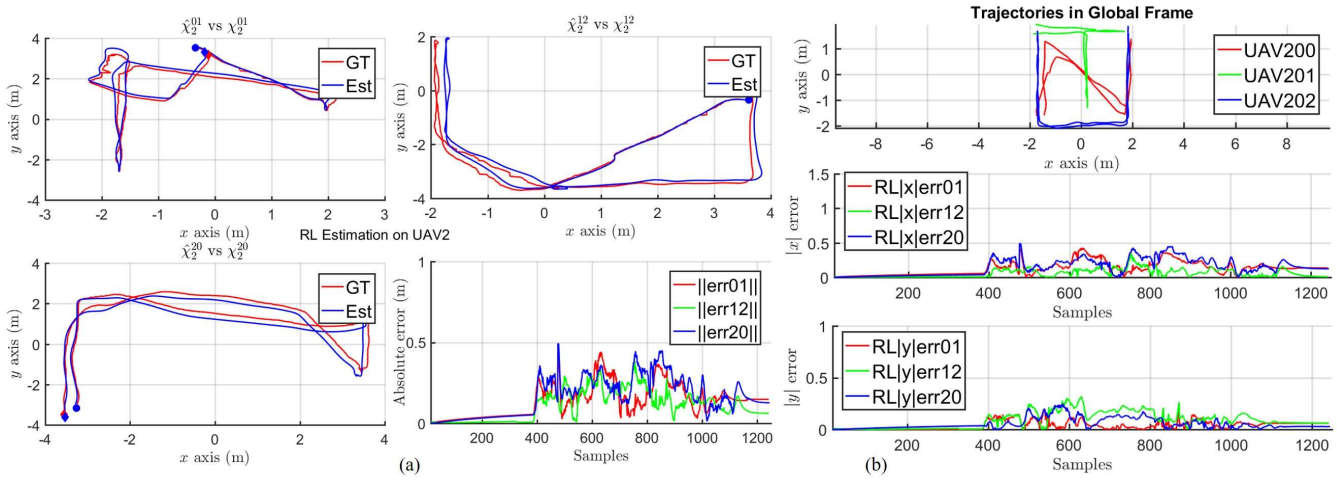

Fig. 7: **Distributed RL estimates of Test** 13 **on each UAV platform:** (a) shows the comparison of RL trajectories calculated on UAV2 and its corresponding 2-norm errors. The RL estimation results on UAV0 and 1 are similar as those on UAV2. **GT** presents the RL ground truth obtained from VICON system and **Est** is the estimation curve. The solid red and blue circles are the starting points of ground truth and RL estimates, and the diamonds represent the corresponding ending points; (b) depicts the global trajectories and absolute RL estimation errors in x and y directions.

Fig. 8: **Video snapshot of 3 UAVs simultaneously estimating relative positions and flying as a formation.** The red circled UAV is a designated leader labelled as 1 and it can be controlled by a pilot to prevent the UAVs from flying towards the crowds. The blue and green circles, labelled as 0 and 2 respectively, are two followers to achieve and maintain a desired formation with the movements of UAV1 (yellow arrow indicates the flight direction of the leader at certain time step). Forward, backward, right and left movements of the formation are demonstrated. In fact, these three UAVs run the same code and no leader is assigned beforehand. Here the designated leader is merely for safety considerations, otherwise the formation centroid may be random due to the perturbations and control accuracy.

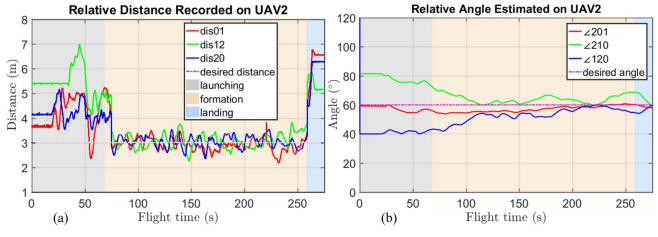

Fig. 9: (a) Inter-UAV distance measurements evolution on each UAV during flight; (b) Bearings of each UAV relative to its neighbors deriving from RL estimates.

[2] S.-M. Kang, M.-C. Park, and H.-S. Ahn, "Distance-based cycle-free persistent formation: Global convergence and experimental test with a group of quadcopters," *IEEE Trans. Ind. Electron.*, vol. 64, no. 1, pp. 380–389, 2017.

[3] X. Dong, Y. Zhou, Z. Ren, and Y. Zhong, "Time-varying formation tracking for second-order multi-agent systems subjected to switching topologies with application to quadrotor formation flying," *IEEE Trans. Ind. Electron.*, vol. 64, no. 6, pp. 5014–5024, 2017.

[4] J. A. Preiss, W. Honig, G. S. Sukhatme, and N. Ayanian, "Crazyswarm: A large nano-quadcopter swarm," in *Proceedings of IEEE International Conference on Robotics and Automation (ICRA)*, May 2017, pp. 3299–3304.

[5] W. Jasim and D. Gu, "Robust team formation control for quadrotors," *IEEE Transactions on Control Systems Technology*, 2017, accepted.

[6] T. M. Nguyen, A. H. Zaini, K. Guo, and L. Xie, "An ultra-wideband-based multi-UAV localization system in GPS-denied environments," in *Proceedings of International Micro Air Vechicle Competition and Conference (IMAV), 2016*, Beijing, China, Oct. 2016, pp. 56–61.

[7] M. Saska, T. Baca, J. Thomas, J. Chudoba, L. Preucil, T. Krajnik, J. Faigl, G. Loianno, and V. Kumar, "System for deployment of groups of unmanned micro aerial vehicles in GPS-denied environments using onboard visual relative localization," *Autonomous Robots*, vol. 41, no. 4, pp. 919–944, 2017.

[8] M. Coppola, K. McGuire, K. Y. Scheper, and G. C. de Croon, "On-board bluetooth-based relative localization for collision avoidance in micro air vehicle swarms," *submitted to Autonomous Robots*, 2016.

[9] S. Wang, D. Gu, L. Chen, and H. Hu, "Single beacon-based localization with constraints and unknown initial poses," *IEEE Trans. Ind. Electron.*, vol. 63, no. 4, pp. 2229–2241, 2016.

[10] K. Guo, Z. Qiu, C. Miao, A. H. Zaini, C.-L. Chen, W. Meng, and L. Xie, "Ultra-wideband-based localization for quadcopter navigation," *Unmanned Systems*, vol. 4, no. 01, pp. 23–34, 2016.

[11] K. Guo, Z. Qiu, W. Meng, L. Xie, and R. Teo, "Ultra-wideband based cooperative relative localization algorithm and experiments for multiple unmanned aerial vehicles in GPS-denied environments," *International Journal of Micro Air Vehicles*, 2017. [Online]. Available: http://journals.sagepub.com/doi/abs/10.1177/1756829317695564

[12] M. Deghat, B. D. Anderson, and Z. Lin, "Combined flocking and distance-based shape control of multi-agent formations," *IEEE Transactions on Automatic Control*, vol. 61, no. 7, pp. 1824–1837, 2016.

[13] B. Dewberry and M. Einhorn, "Indoor aerial vehicle navigation using ultra wideband active two-way ranging," 2016.

[14] G. Chai, C. Lin, Z. Lin, and W. Zhang, "Consensus-based cooperative source localization of multi-agent systems with sampled range measurements," *Unmanned Systems*, vol. 2, no. 03, pp. 231–241, 2014.